Piezoelectric Photoacoustic Evaluation of Si Wafers with Buried Structures

Yao-Chun Shen, *Student Member, IEEE*, and Shu-Yi Zhang, *Senior Member, IEEE*

Abstract — **The piezoelectric photoacoustic evaluation of Si wafers with buried structures is studied experimentally and theoretically. In the experiment, we have detected and imaged the Sb-doped regions in a Si wafer covered by an epitaxial Si layer with about 10 μm thickness. On the other hand, in order to explain the experimental results, the one-dimensional (1-D) multilayered model with discontinuous thermal impedance between the neighboring layers is used and the expressions for the thermal and acoustic fields in the sample and PZT transducer are also presented. Moreover, the numerical calculations in accordance with the practical experimental conditions have been carried out and the theoretical results are in agreement with those of experiment.**

I. Introduction

IT IS WELL KNOWN that the doped regions in Si wafers, which may be invisible by optical microscope, can be easily detected and imaged by thermal wave microscope [1]. In addition, using photoacoustic microscopy (PAM), the depth profiling of multilayered structures, specially the semiconductor materials and devices, can be detected by either changing the modulation frequency or adjusting the phase angle shift, and even by correlation photoacoustic (PA) technique [2]–[4]. Generally, PA measurements can be performed by microphone and piezoelectric transducer, either contact or noncontact (i.e., air transducer). The contact detection system, in which the piezoelectric transducer is bonded with sample, is usually adopted in PAM because of its high sensitivity and resolution.

On the other hand, since White [5] analyzed the elastic wave generation in isotropic elastic bodies by an electron beam or electromagnetic energy, a quite number of authors have already proposed some different theoretical models for investigating the mechanisms of PA detection and depth profiling of thermal wave imaging in condensed materials. For multilayered materials, Opsal and Rosencwaig [6] developed a 1-D model of thermal wave depth profiling in which they considered a semi-infinite elastic body with discontinuous thermal impedance between two neighboring layers. At the same time, Zhang and Chen [2] suggested a simplified 1-D theory in accordance with their practical experimental conditions in which an analytical expression of the PA signal induced by the thermoelastic effect of the sample has been obtained. Using the simplified theory, the experimental results of the laminated imaging obtained by adjusting the phase shift in piezoelectric PA detection can be qualitatively explained, but the thermal inhomogeneities of the sample has not been taken into account in the theory.

Manuscript received January 29, 1991; revised and accepted July 31, 1991. This work was supported by the Natural Science Foundation of China under grant 18974028.

The authors are with the Laboratory of Photoacoustic Sciences, Institute of Acoustics, Nanjing University, Nanjing 210008 China.

IEEE Log Number 9105559.

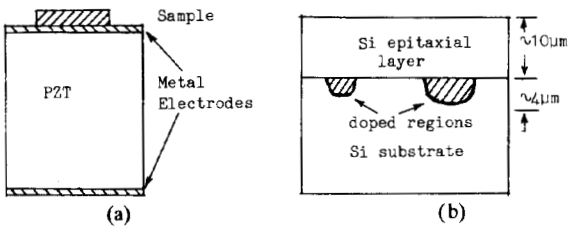

Fig. 1. (a) Configuration of transducer-sample geometry. (b) Depth structures of the sample.

In this paper, based on the results of Opsal *et al.* [6] and Zhang *et al.* [2], the piezoelectric PA detection of the multilayered sample with discontinuous thermal impedance and thermal thick but acoustical thin conditions has been investigated in both experiment and theory. In the experiment, using a contact piezoelectric PAM system, we have detected and imaged some multilayered semiconductor samples, especially the Si wafers with buried structures. On the other hand, the distributions of the thermal and acoustic fields in the sample and PZT transducer have been calculated theoretically. The good agreement between the theoretical and experimental PA signals is obtained. Both show that the suitable modulation frequency and phase shift should be chosen for getting the high contrast PA images to reflect some interesting subsurface features.

II. Experiment

In the contacted piezoelectric PAM system as described by Zhang *et al.* [2], a cylindrical PZT transducer with longitudinal vibration mode is bonded on the back of the sample (see Fig. 1(a)). The output voltage of the PZT transducer is amplified by a preamplifier and a lock-in amplifier. The different PA images can be obtained by adjusting the phase shift angle of the reference signal that must be provided to lock-in amplifier for improving signal to noise ratio.

In order to study the mechanism of the laminated imaging by PAM, some multilayered semiconductor samples have been prepared. Fig. 1(b) shows a silicon wafer with Sb-doped regions covered by an epitaxial Si layer about 10 μm thickness. A series of PA images displaying the doped areas at different phase shifts are shown in Fig. 2, where the original phase shift between the modulated optical beam and the reference signal has already been subtracted. The dark areas in Fig. 2 are corresponding to the Sb-doped regions and the

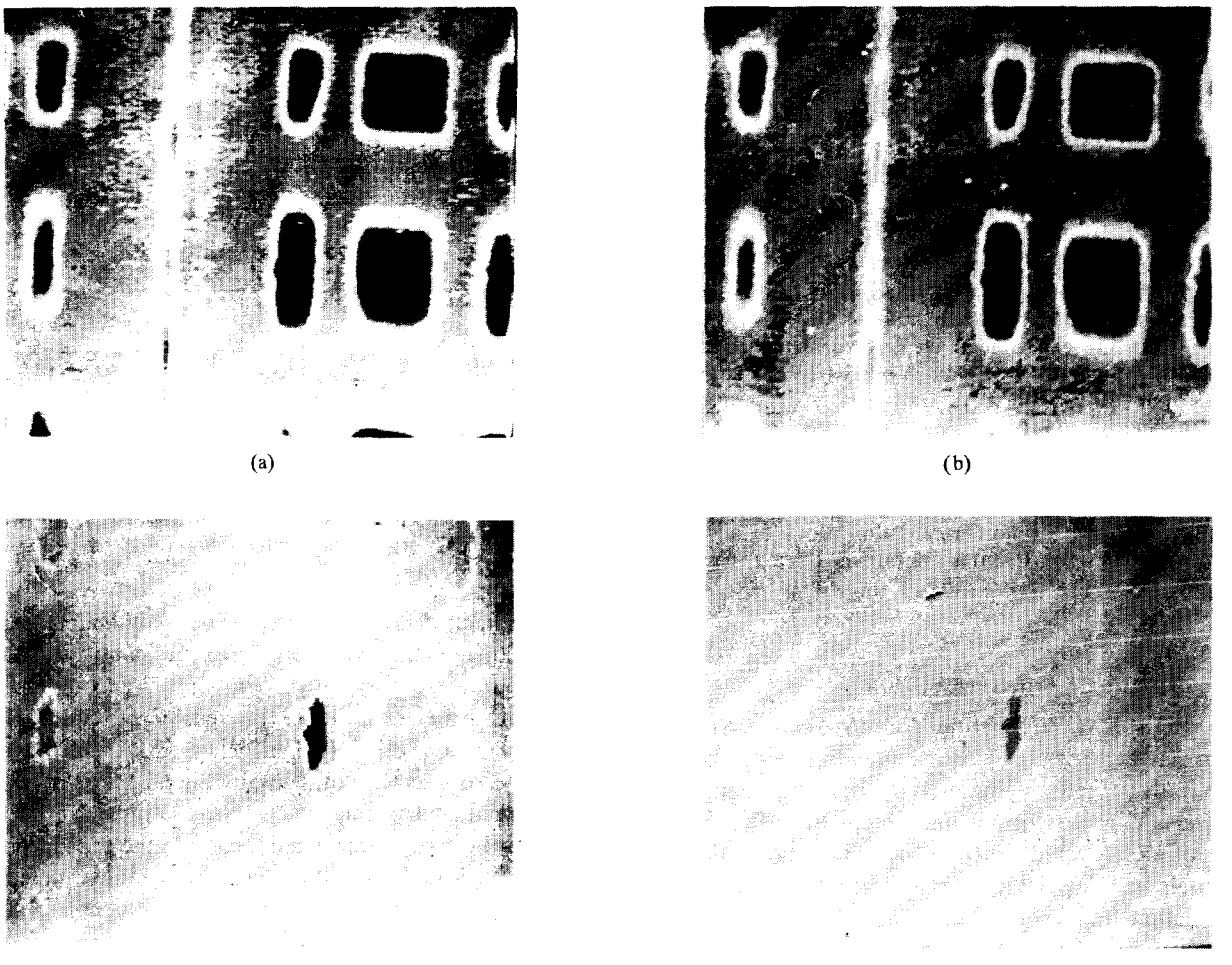

Fig. 2. PA images in frequency 10 kHz at different phase shifts: (a) 160°. (b) 209°. (c) 215°. (d) 220°.

white circumferences may reflect the transverse $p-n$ junctions between doped and nondoped regions. It can also be seen from Fig. 2 that the larger phase shift corresponds to larger depth since the doped regions at deeper position occupy smaller areas. As the phase shift increases continuously, the images of the doped areas will completely disappear.

The experiment has been performed at different modulation frequencies. The results show that the PA signal decreases as frequency increases, but the more detailed structures may be displayed at the higher modulation frequencies. It is obviously illustrated that the higher operating frequency gives much higher resolution. The experiment has also been performed under different boundary conditions. Comparing the results obtained under the mechanical free boundary and the mechanical constrained boundary conditions, the latter provides less or even no information of subsurface layers although it gives more than ten times larger PA signal.

III. Theory

A laser beam with modulated intensity is incident upon the surface of the multilayered sample as shown in Fig. 3. It is assumed that 1) the sample is opaque and the absorption of light only occurs at the surface of the sample. 2) the sample is thermal thick but acoustical thin and the acoustic wave vector

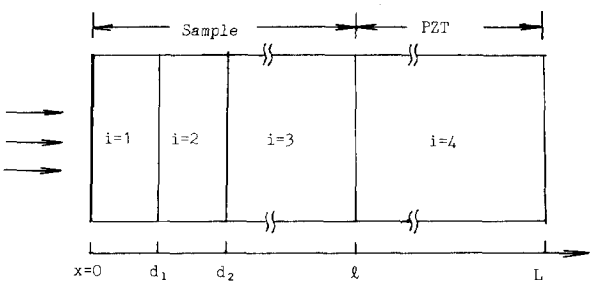

Fig. 3. One-dimensional multilayered model.

of the sample is the same as that of PZT transducer. 3) the sample is uniform in transverse but multilayered with discontinuous thermal impedance in depth direction. Therefore, for simplicity, a 1-D multilayered model is used [2]–[6].

A. Thermal Wave Field

In accordance with the sample used in the experiment, a three-layered model is considered. Then the 1-D heat diffusion equation in ith layer is

$$\frac{d^2T_i}{dx^2} - q_i^2 T_i = 0 \qquad (i = 1, 2, 3) \tag{1}$$

where T_i and q_i are the temperature and the thermal wave vector of the ith layer respectively, $i = 1, 2, 3$ represent the first, second and third layer of the sample, and

$$q_i = (1 - j)/u_i, \quad u_i = (2K_i/\omega\rho_i C_i)$$

where ω is the modulation frequency of the laser beam, ρ_i, C_i, K_i are the density, specific heat and thermal conductivity of the ith layer of the sample respectively.

Since the thickness of the sample is much larger than the thermal wavelength of the sample, the thermal wave can be ignored in the PZT transducer. Then the boundary conditions can be written as

$$-K_1 dT_1/dx = Q \qquad (x = 0) \qquad (2a)$$

$$T_1 = T_2,\ K_1 dT_1/dx = K_2 dT_2/dx \qquad (x = d_1) \qquad (2b)$$

$$T_2 = T_3,\ K_2 dT_2/dx = K_3 dT_3/dx \qquad (x = d_2) \qquad (2c)$$

where Q is the heat flow produced at the surface of the sample. From (1) and (2) we can get

$$\begin{aligned} T_1(x) &= A[\exp(-q_1 x) + \Gamma_1 \exp(q_1 x)] \qquad (0 < x < d_1) \\ T_2(x) &= B[\exp(-q_2 x) + \Gamma_2 \exp(q_2 x)] \qquad (d_1 < x < d_2) \\ T_3(x) &= C \cdot \exp(-q_3 x) \qquad (d_2 < x < l) \end{aligned} \tag{3}$$

where the coefficients A, B, C, Γ_1, and Γ_2 can be determinated as follows:

$$\begin{aligned} A &= Q/Z_1(1 - \Gamma_1) \\ B &= A[\exp(-\alpha_{11}) + \Gamma_1 \exp(\alpha_{11})]/ \\ &\quad [\exp(-\alpha_{21}) + \Gamma_2 \exp(\alpha_{21})] \\ C &= B[\exp(-\alpha_{22}) + \Gamma_2 \exp(\alpha_{22})]/\exp(-\alpha_{32}) \\ \Gamma_1 &= \exp(-2\alpha_{11})[(1 - \Gamma_2)Z_2 - (1 + \Gamma_2)Z_1]/ \\ &\quad [(1 - \Gamma_2)Z_2 + (1 + \Gamma_2)Z_1] \\ \Gamma_2 &= \exp(2\alpha_{22} - 2\alpha_{21})(Z_3 - Z_2)/(Z_3 + Z_2) \end{aligned}$$

where

$$Z_i = K_i q_i, \quad \alpha_{ij} = q_i d_j \quad (i, j = 1, 2, 3).$$

B. Elastic Wave Field

In the 1-D approximation, only longitudinal elastic mode needs to be taken into account. Then the thermoelastic wave equation in the different layers of the sample and the PZT transducer is

$$\frac{d^2\phi_i}{dx^2} + k^2\phi_i = f(x) \qquad (i = 1, 2, 3, 4) \tag{4}$$

where ϕ_i is the elastic displacement potential and k is the acoustic wave vector, $i = 4$ represents the PZT transducer, and

$$f(x) = \gamma_i T_i(x)$$

where $T_i(x)$ is the thermal field given above and γ_i is the thermoelastic constant defined as

$$\gamma_i = \alpha_{ti}(2\mu + 3\lambda)/(2\mu + \lambda)$$

where λ and μ are the Lamé constants, α_{ti} is the thermal expansion coefficient of ith layer of the sample.

The solution of (4) can be expressed by Green function

$$\phi(x) = \int_o^\ell G(x, x') f(x')\, dx'. \tag{5}$$

The Green function $G(x, x')$ describes the elastic response at x due to a delta function source at x' and satisfies the following equation

$$\frac{\partial^2 G}{\partial x^2} + k^2 G = \delta(x - x'). \tag{6}$$

The displacement u and the stress σ can be written as

$$\begin{aligned} u &= d\phi/dx \\ \sigma &= -(2\mu + \lambda)k^2\phi. \end{aligned} \tag{7}$$

If the surface of the sample and the bottom of the transducer are free, then the boundary conditions are

$$\sigma(0) = 0,\ \sigma(L) = 0 \quad \text{(free boundary)} \tag{8a}$$

and if the surface of the sample is constrained and the bottom of the transducer is free, the boundary conditions are

$$u(0) = 0,\ \sigma(L) = 0 \quad \text{(constrained boundary)}. \tag{8b}$$

The solution of (6) with boundary conditions (8) is obtained as follows

$$G(x, x') = \begin{cases} 2\displaystyle\sum_{n=1}^{\infty} \sin(a_n x)\sin(a_n x')/\left(k^2 - a_n^2\right)L \\ \qquad \text{(free boundary)} \qquad (9a) \\ 2\displaystyle\sum_{n=1}^{\infty} \cos(b_n x)\cos(b_n x')/\left(k^2 - b_n^2\right)L \\ \qquad \text{(constrained boundary)} \qquad (9b) \end{cases}$$

where

$$a_n = n\pi/L, \qquad b_n = (2n - 1)\pi/2L.$$

According to piezoelectric equation, the electric field intensity E can be written as

$$E = -h\frac{\partial u}{\partial x} \tag{10}$$

where h is the piezoelectric coefficient of the PZT. The output voltage of PZT induced by the heat source at x' is the integral of $E(x, x')$ with respect to x:

$$V(x') = \int_\ell^L E(x, x')\, dx$$

that is

$$V(x') = \begin{cases} 2hk^2 f(x') \sum_{n=1}^{\infty} \dfrac{\sin(a_n x')}{k^2 - a_n^2} \displaystyle\int_{\ell}^{L} \sin(a_n x)\, dx \\ \qquad \text{(free boundary)} \qquad (11a) \\ 2hk^2 f(x') \sum_{n=1}^{\infty} \dfrac{\cos(b_n x')}{k^2 - b_n^2} \displaystyle\int_{\ell}^{L} \cos(b_n x)\, dx \\ \qquad \text{(constrained boundary).} \qquad (11b) \end{cases}$$

If the PZT transducer is operated near the resonance frequency, only the nth term in the summation should be taken into account. Moreover, the thermal wavelength is much smaller than the thickness of the sample, thus $x' \ll L$ and $\sin(a_n x')$ approaches to $a_n x'$ and $\cos(b_n x')$ tends to 1. As n is not very large, a good approximation of (11) is

$$V(x') = \begin{cases} 2a_n k^2 x' f(x') / (k^2 - a_n^2) L \cdot \displaystyle\int_{\ell}^{L} \sin(a_n x)\, dx \\ \qquad \text{(free boundary)} \qquad (12a) \\ 2k^2 f(x') / (k^2 - b_n^2) L \cdot \displaystyle\int_{\ell}^{L} \cos(b_n x)\, dx \\ \qquad \text{(constrained boundary).} \qquad (12b) \end{cases}$$

From (12), the PA signal due to the heat source at x' can be derived. The PA signal is proportional to $x'f(x')$ for free boundary or proportional to $f(x')$ for constrained boundary.

The detected electric signal, i.e., the total output of PZT, is the integral of $V(x')$ with respect to x'. In addition, the integral of $f(x')$ with respect to x', as x' from 0 to ℓ, is independent of the thermal conductivity of the subsurface layer of the sample. Therefore, we can deduce that the thermoelastic signal under the constrained boundary provides no information of the subsurface layers if the sample is inhomogenous only in the thermal conductivity. However, such information can be provided under the free boundary where the thermoelastic signal is the integral of $x'f(x')$ with respect to x'. Moreover, since an $x' \ll 1$, the PA signal under the free boundary is much smaller than that under the constrained boundary. All of these results are consistent with the phenomena observed in the experiment.

In order to improve the signal to noise ratio, the PA signal is generally mixed with a reference signal

$$V_r = 2\cos(\omega t + \Psi)$$

where Ψ is the phase shift of the reference signal. The imaging signal is the dc component of the mixed signal.

$$V_i(x') = V(x') \cdot \exp(-j\Psi)$$

then the subsurface structures that needs to be detected can be displayed conspicuously in the PA imaging by adjusting the phase angle shift of the reference signal.

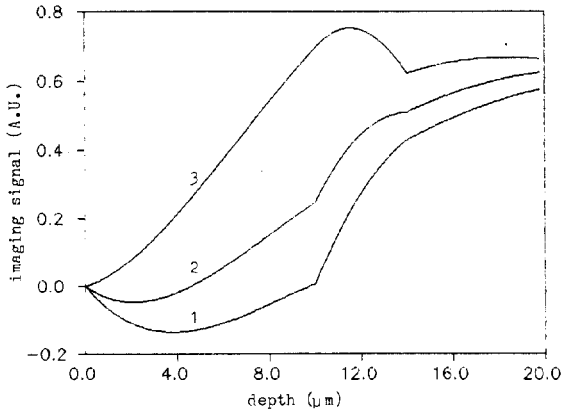

Fig. 4. Imaging signal contributed by the heat source at depth x' as different phase shifts: (1) 0°. (2) 45°. (3) 60°.

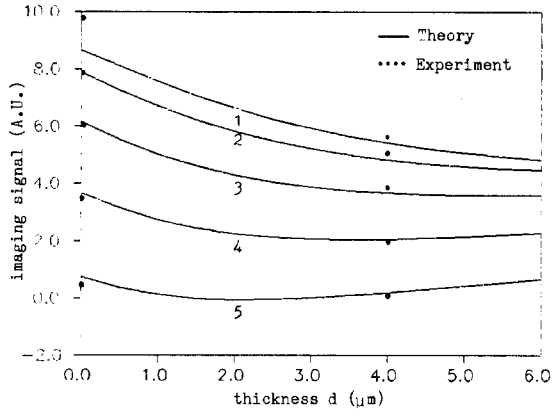

Fig. 5. Imaging signal versus thickness d of buried layer at different phase shifts. (1) 50° . (2) 70°. (3) 90°. (4) 110°. (5) 130°.

IV. Numerical Results and Discussion

In order to compare the theoretical and experimental results, using the theoretical equations and the experimental conditions described previously, the numerical calculations have been done with the parameters taken from [10].

A. $V(x')$ Versus x'

The curves shown in Fig. 4 are obtained with different phase shifts. It is indicated that $V(x')$, the imaging signal from the thermal sources at depth x', changes with the phase shift. Thus we can deduce that the contribution of a section layer of the sample to the imaging signal can be weakened or strengthened by changing phase shift, then the important depth profiling capability is provided by PAM.

B. PA Signal versus Thickness d of the Buried Layer

The PA signal varying with the thickness d of the buried layer at different phase shift are shown in Fig. 5. From the curves we can see that the additional PA signals of doped areas gradually decrease as phase shift increases from 50° to 130°, this is consistent with the measured results.

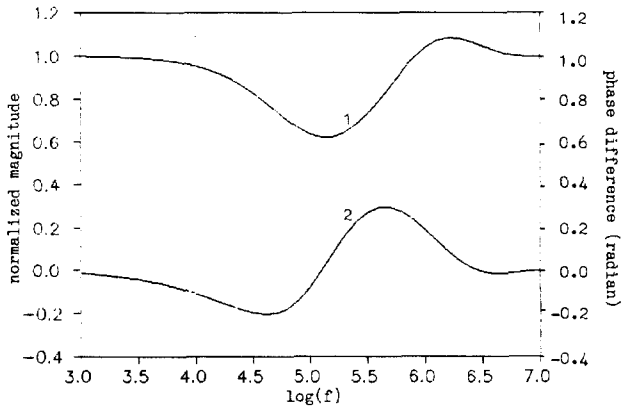

Fig. 6. PA signal versus frequency. (1) Normalized magnitude. (2) Phase difference.

C. PA Signal versus Frequency

Generally, the PA signal of Si wafers decreases as frequency increases. In order to evaluate the additional PA signal induced by the doped impurity, the influence of the frequency dependence of Si substrate on the additional PA signal must be eliminated. In Fig. 6, the frequency dependence of the amplitude ratio A_d/A_s and the phase difference $\Psi_d - \Psi_s$ are shown respectively, where A_m and Ψ_m are amplitude and phase of the PA signal, and $m = s, d$ are corresponding to Si substrate and doped areas respectively. The curves show that both amplitude and phase shift can not provide information about the buried layer if the modulation frequency is very high or very low. It can be explained as follows. 1) At very high frequency, the epitaxial Si layer can be considered as thermal thick, therefore, the PAM can not "see" the buried layer since no thermal wave penetrates it. 2) At very low frequency, both epitaxial Si layer and buried layer can be considered as thermal thin, hence the PA signal comes mainly from the third layer, i.e., Si substrate, and the contribution of the buried layer can be neglect. So in these two cases, the buried layer can not be detected by PAM. Moreover, there are two additional factors affect the quality of the PA images. 1) PA signal to noise ratio decreases at high frequency. 2) The resolution of PA images reduces at low frequency. Thus the optimum value of modulation frequency ensures that the thermal diffusion length approximates the total thickness of the epitaxial layer and the buried layer. In our case, the proper modulation frequency is about 100 kHz.

V. Conclusion

The experiment results show obviously that the piezoelectric PAM is a useful technique for evaluating the buried structures, which are difficult to be inspected by other microscopes, such as optical or electron microscopes. In order to detect apparently the buried structures, the modulation frequency must be selected carefully. Generally, it is required that the thermal diffusion length approximates to the total thickness of the epitaxial layer and the buried layer.

References

[1] A. Rosencwaig and R. M. White, "Imaging of dopant regions in silicon with thermal-wave electron microscopy," *Appl. Phys. Lett.*, vol. 38, pp. 165–167, 1981.

[2] S. Y. Zhang and L. Chen, "Photoacoustic microscopy and detection of subsurface features of semiconductor devices," in *Photoacoustic and Thermal Wave Phenomena in Semiconductors*, A. Mandelis, Ed. New York: Elsevier Science, 1987, pp. 27–52.

[3] L. H. Wei, J. S. Xu, and S. Y. Zhang, "Application of two-dimensional Hadamard transform to photoacoustic microscopy," *IEEE Ultrason. Symp. Proc.*, 1986, pp. 501–504.

[4] S. Y. Zhang, Q. Shen, B. Yan, Z. Q. Wang, and Y. C. Shen, "Depth profiling of opaque multilayer materials by correlation photoacoustics," in *Springer Series in Optical Science*, vol. 58, *Photoacoustic and Photothermal Phenomena II*, J. C. Murphy *et al.*, Eds. New York: Springer-Verlag, 1990, pp. 67–70.

[5] R. M. White, "Generation of elastic waves by transient surface heating," *J. Appl. Phys.*, vol. 34, pp. 3554–3567, 1963.

[6] J. Opsal and A. Rosencwaig, "Thermal-wave depth profiling: Theory," *J. Appl. Phys.*, vol. 53, pp. 4240–4246, 1982.

[7] W. Z. Shen, *Handbook of Applied Integrated Circuit Technique*, 1989 (in Chinese).

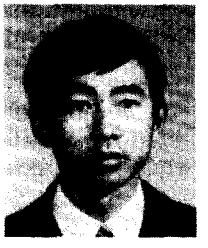

Yao-Chun Shen (S'88) was born in Jiangsu, China, on March 19, 1965. He received the B.S. degree in physics and M.S. degree in radio physics, both from Nanjing University, Nanjing, China, in 1986 and 1989 respectively. He is currently working toward the Ph.D. degree in the Institute of Acoustics, Nanjing University. His current research interests include photoacoustics and scientific applications to solid state materials and devices.

Shu-Yi Zhang (M'86–SM'88) was born in Zhejiang, China. She graduated from the Physics Department of Nanjing University, Nanjing, China, and then from the graduate school of the same university with a specialty in acoustics.

She is a Professor and the Director of Photoacoustic Sciences Laboratory, Institute of Acoustics, Nanjing University, where she has been working on molecular acoustics, low-temperature acoustics, surface acoustic waves, acoustic-optic interaction and photoacoustic sciences. She also has been a Visiting Associate Professor of the Physics Department of Wayne State University, Detroit, MI, in 1985, and a Professor of Ecole Superieure de Physique et de Chimie de la Ville de Paris, France, in 1988.

Dr. Zhang is a member of the Chinese Society of Physics, the Chinese Society of Electronics, the Chinese Society of Optics, and the Standing Committee of the Chinese Society of Acoustics.